Current stress and switching loss evaluation of a unified expandable power converter used for grid-integration of renewable energy sources

Bizhani, Hamed; Muyeen, S.M.; Tatari, Fatemeh R.; Techato, Kuaanan; BenBrahim, Lazhar; Blaabjerg, Frede

Published in:
IET Renewable Power Generation

DOI (link to publication from Publisher):
10.1049/rpg2.12148

Publication date:
2021

Document Version
Publisher's PDF, also known as Version of record

Received: 4 January 2021 | Revised: 15 February 2021 | Accepted: 24 February 2021

IET Renewable Power Generation

DOI: 10.1049/rpg2.12148

The Institution of Engineering and Technology WILEY

ORIGINAL RESEARCH PAPER

Current stress and switching loss evaluation of a unified expandable power converter used for grid-integration of renewable energy sources

Hamed Bizhani[1,2] | **S. M. Muyeen**[3] | **Fatemeh R. Tatari**[4] | **Kuaanan Techato**[5] | **Lazhar Ben-Brahim**[6] | **Frede Blaabjerg**[7]

[1] Department of Electrical Engineering, University of Zanjan, Zanjan, Iran

[2] Sun-Air Research Institute, Ferdowsi University of Mashhad, Mashhad, Iran

[3] Department of Electrical Engineering, Curtin University, Perth, Australia

[4] Electrical Engineering Department, Shahrood University of Technology, Shahrood, Iran

[5] Faculty of Environmental Management, Prince of Songkla University, Songkhla, Thailand

[6] Department of Electrical Engineering, Qatar University, Doha, Qatar

[7] Department of Energy Technology, Aalborg University, Aalborg, Denmark

Correspondence
Hamed Bizhani, Department of Electrical Engineering, University of Zanjan, Zanjan, Iran.
Email: hamedbizhani@znu.ac.ir

Abstract

Due to the intermittent nature of the renewable energy systems (RESs), more specifically, solar panels and wind turbines, their sole use does not lead to a smooth and reliable power. To overcome this issue, the concurrent grid-integration of RESs to form a microgrid is reported. In the DC-bus microgrid, the produced power by RES is initially given to the shared DC-bus through an individual source-side converter and then transmitted to the utility via a common grid-side converter. By increasing the number of RESs, the number of required power converters, and therefore, the investment cost also increase. Using the cost-effective multi-input low-switch converters is a promising alternative to alleviate this significant need for individual converters. Recently, a nine-switch-based unified expandable power converter (UEPC) has been presented for concurrent integration of AC and DC sources with a tangible fewer switch count. This unified structure has been utilized in two configurations named AC-AC-AC and AC-AC-DC. In this paper, both configurations are evaluated and compared in terms of current stress and switching loss. Considering the current stress analysis, the best port for interfacing with the grid to lower the total current rating of power switching devices is also determined. The high-performance capability of both configurations is finally verified using MATLAB/Simulink.

1 | INTRODUCTION

Renewable energy-based distributed generation systems are the most promising solution to overcome the environmental issues and facing with depleting of the fossil fuel reserves [1]. Wind energy system (WES) and solar energy system (SES) are two well-known RESs for generating clean electrical energy from the wind and sun, respectively. Despite the remarkable features of these clean energy systems, they suffer from the intermittent power generation caused by their high dependency to the weather conditions [2]. Therefore, the individual use of an RES with uncertainty in its output power leads to an unreliable and non-programmable power, restricting its sole utilization especially in off-grid operation mode [3]. To overcome this problem, the concurrent utilization of different numbers and types of RESs in the form of microgrid is reported in the literature to enhance the system's reliability [4].

In a conventional microgrid as shown in Figure 1, the produced power by RESs and other distributed generations are first converted and given to DC-bus. The DC and AC loads are then supplied by DC-bus through individual power electronics interfaces. As it can be seen, enormous power converters with different functionality are needed to manage power flow between sources and loads, increasing the investment cost of the system [5]. To lower this, the multi-port power electronics interfaces in which several sources can be united using a unified structure are introduced in the literature [6–14]. DC-DC multi-port converters are the most well-known converters being presented for the integration of DC-based RESs [15]. The union of AC and DC-based RESs is also feasible through DC-DC multi-port

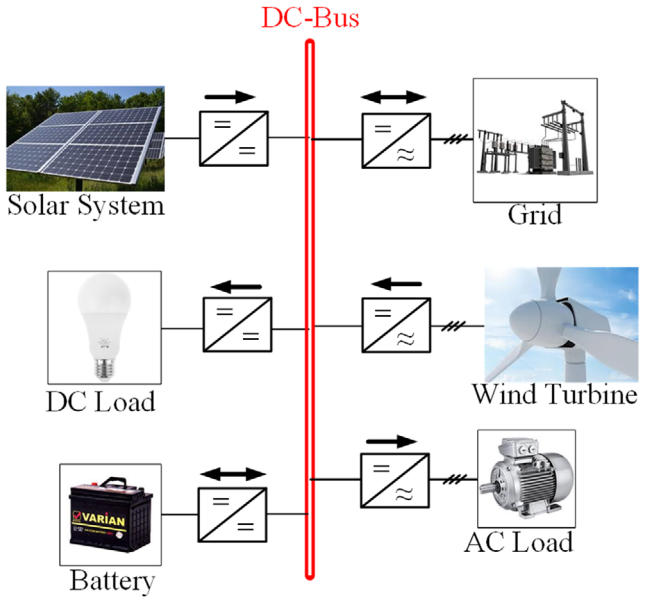

FIGURE 1 Conventional microgrid strucure based on individual converters

converters. For this aim, an uncontrollable rectifier is also utilized to convert AC voltage of AC-based RES to a DC voltage and its connection to the multi-port converter [16]. In the literature, several power electronic interfaces have been also proposed to reduce the number of semiconductors used in WES applications [6–9]. In [6], a five-leg converter is replaced with the back-to-back (B2B) converter in doubly fed induction generator (DFIG) based WESs to achieve the same functionality with reduced switch count. A nine-switch converter (NSC) enjoying three lower switches in comparison to B2B structure, is reported in [7] and [10, 11] for grid-connection of a permanent magnet synchronous generator (PMSG) based WES and a DFIG based WES, respectively. A modified version of nine-switch converter with six switches is presented in [8]. The switches located in the third leg of the NSC are replaced with three capacitors in that structure. In [9] a compact topology, which is a developed version of the NSC, is presented for the integration of distributed generation systems. Different feasible configurations of presented topology in [9], are analyzed in [12] in order to handle different distributed generation systems combinations. All the above-mentioned topologies are only used for the integration of a limited number of renewable energy resources. To cover this limitation, a sequential space vector modulation (SSVM) based unified power electronic converter (UEPC), which significantly reduces the number of switches in comparison to the conventional structure, is proposed in [13]. In UEPC, n PMSG based WESs can be integrated into the grid while the grid port is shared between all PMSGs. Considering a few substantial modifications in the structure and modulation of the UEPC, a generalized expandable nine-switch based converter, which is able to integrate both AC- and DC-based renewable energy resources, is proposed in [14]. Three independent photovoltaic systems along with a PMSG based WES are unified using the proposed converter. Although the UEPC enjoys several advantages such as lower switch count, compactness, and plug and play capability, the total required current rating of the semiconductors seems high caused by shared switches in the UEPC structure. To make an accurate conclusion in this regard, a current stress analysis should be considered. In addition, considering two feasible AC-AC-AC and AC-AC-DC configurations for UEPC, the switching loss evaluation of UEPC would be useful to highlight the advantage and disadvantages of every configuration. In this paper, to determine the total required current rating of the UEPC, different feasible configurations according to the location of the shared grid side port are obtained, and the best port that imposes a lower rating for switches is proposed. A deep switching loss evaluation is then given to compare both AC-AC-AC and AC-AC-DC configurations to provide a guideline for different applications. The high performance of both configurations is finally verified using MATLAB/Simulink software.

2 | UNIFIED CONFIGURATION DESCRIPTION

2.1 | Architecture

In a conventional microgird configuration depicted in Figure 1, 18 power switching devices are required, which is 6 (33%) switches more than the compact structure reported in [14]. The unified configuration with lower power switching devices count for the interconnection of different types of renewable energy sources and loads in a DC-bus based microgrid, is represented in Figure 2. As can be seen, this unified converter can be used in two configurations named AC-AC-AC (Figure 2(a)) and AC-AC-DC (Figure 2(b)). In the former one, the AC-based RESs are only integrated [13]. However, in AC-AC-DC, the upper ports interface with AC sources and loads, whereas the lower port of every phase is used for interfacing with DC sources, storage systems, and DC loads [14]. In the generalized type of the compact converter, n AC sources and loads along with m DC sources and loads can be integrated into the main grid. As it is depicted in Figure 2(b), by using four power switching devices in each leg, one AC source, one DC source, one DC load, and one storage can be united. All semiconductor switches in the compact structure are bidirectional, which means bidirectional power exchange between every port and DC-bus is inherently available. As a DC-bus microgrid, the generated power of AC sources is given to DC-bus via AC-to-DC conversion although the AC loads absorb active power from DC-bus through DC-to-AC conversion. On the other hand, the produced power by DC sources is given to DC-bus via a step-up DC-DC conversion and the demanded power by DC loads is provided using a step-down DC-DC conversion. It is noted that storage systems can also be connected to DC port. During the charging mode, the storage is being charged through a step-down DC-DC conversion. However, the storage is being discharged via a step-up DC-DC conversion during discharging mode. It is worth mentioning that the battery necessarily needs a bidirectional DC-DC conversion. It can be connected to every DC port because all DC ports enjoy a bidirectional inherent characteristic that makes

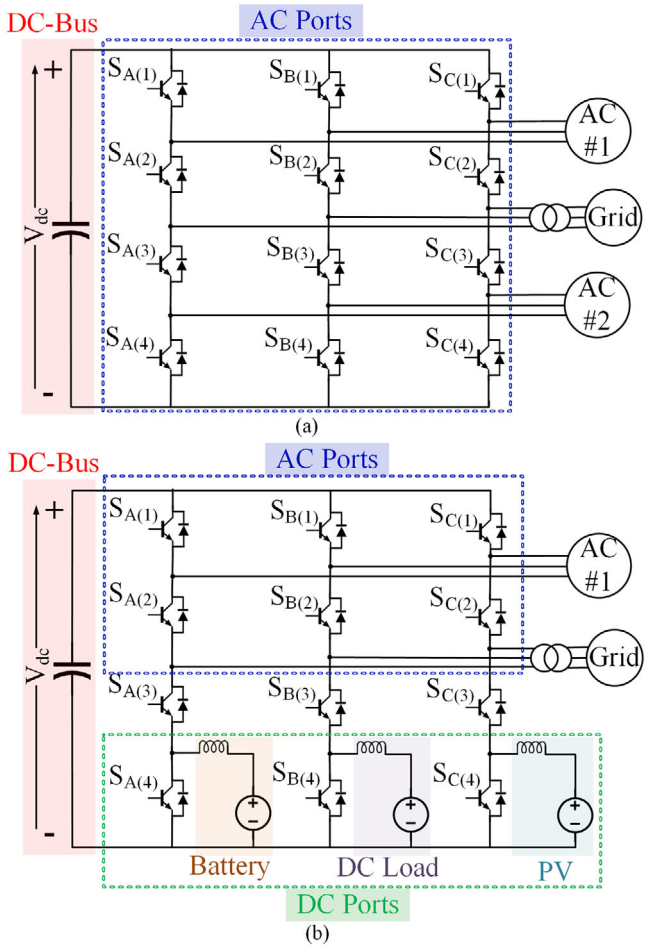

FIGURE 2 Unified structure for compact grid-integration of RESs, (a) AC-AC-AC configuration, and (b) AC-AC-DC configuration

the second configuration a suited topology for off-grid operation.

In this paper, two above-mentioned configurations are taken into account for current stress and switching loss evaluation. For this aim, the instantaneous current passing through every switch located in every phase is first calculated. Then, considering the DC and AC sources' currents, the instantaneous currents are updated. Finally, according to the current analysis of a nine-switch converter [17, 18], the switching loss evaluation of both configurations is given.

2.2 | Sequential space vector modulation

In the conventional configuration shown in Figure 1, all converters work individually with separate control and modulation subsystems. In the proposed compact microgrid, the physical dependency of the converter limits the individual performance of the connected AC and DC sources. To alleviate this limitation, a sequential space vector modulation is reported [13, 14, 19]. In this switching scheme, every AC and DC port is treated as an individual converter to obtain its feasible switching states. The switching period is divided into two intervals. At the first interval, the individual switching states of AC ports are sequentially applied. During this interval, all DC ports will automatically be in charging or discharging mode. If a source is connected to the DC port, it works in charging mode while the switching states of AC ports are being applied. Otherwise, if a load is connected to DC port, it works in discharging mode while the switching states of AC ports are being applied. At the second interval, considering the mutual effect of the switching states of AC ports on the DC ports, the duty cycle of every DC port is updated and then, the corresponding pulse is applied. It is worth mentioning that while the pulse signals of DC ports are being applied, all AC ports work in zero mode, which means there is no power exchange between DC-bus and AC ports. The reader is referred to [14] for further details about sequential space vector modulation for unified converter.

In the conventional microgrid, the DC-bus and its energy are available for every individual source/load during the entire switching period. Therefore, the energy can be exchanged between DC-bus and source/load as long as the switching period. However, in the compact microgrid, DC-bus and its energy are only accessible for every port as long as its corresponding time interval. Therefore, the energy can only be exchanged between every port and DC-bus in a part of switching period. This limitation leads to a lower total energy exchange capability for every source/load that also deteriorates the control system performance. To avoid this, the switching frequency needs to be lower in comparison to the conventional topology, which causes a higher harmonic distortion in output's currents and voltages. Since the total exchanged energy is proportional to voltage and time, as an alternative way, DC-bus voltage can be designed to be larger to meet the required energy exchange ratio. In this paper, the DC-bus voltage in the compact microgrid is set to 1500 V for covering this issue.

3 | CURRENT STRESS ANALYSIS

3.1 | Instantaneous current

The instantaneous current flowing through every switch in each phase depends on the switching state of the leg and connected sources' current. Considering the sequential space vector modulation, it is obvious that in every switching state, only one switch has to be OFF. Assuming the direction for different configurations as depicted in Figure 3, the instantaneous current passing through switches in phase A, can be tabulated as Table 1, where i_D can be either I_{DC} or i_{S2}. It is noted that phases B and C experience the same conditions, therefore, the evaluation is only performed for phase A. As it can be seen, depending on the switching state, each switch might experience different instantaneous current. Considering the same direction, phase and frequency for all outputs, the upper and lower switches experience the highest current although the middle switches experience lower instantaneous current. However, according to the current analysis presented in [17, 18] for an NSC, the instantaneous current magnitude and therefore the conduction loss, depends on the polarity, phase, and frequency of all components. This means in

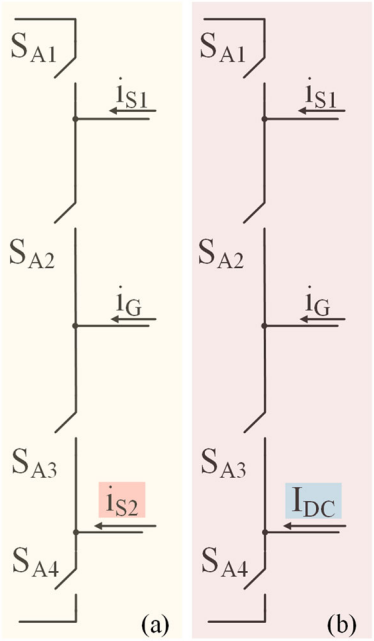

FIGURE 3 Current direction in (a) AC-AC-AC and (b) AC-AC-DC configurations

TABLE 1 Instantaneous currents for a three-port version of UEPC considering different switching states

	S_{A1}=OFF	S_{A2}=OFF	S_{A3}=OFF	S_{A4}=OFF
i_{SA1}	0	$-i_{S1}$	$-(i_{S1}+i_G)$	$-(i_{S1}+i_G+i_D)$
i_{SA2}	i_{S1}	0	$-i_G$	$-(i_G+i_D)$
i_{SA3}	$(i_{S1}+i_G)$	i_G	0	$-i_D$
i_{SA4}	$(i_{S1}+i_G+i_D)$	(i_G+i_D)	i_D	0

some applications such as uninterruptible power supply (UPS), the instantaneous current and conduction loss can be low.

3.2 | Current rating of semiconductors

In the grid integration, the RESs inject power to the DC link although the grid absorbs power from the DC-link. This means the currents of RESs are in an opposite direction with the grid side current. Considering nominal current of each RES equal to I, the nominal current in the grid side is equal to $2I$. As summarized in Table 2, when the grid is connected to the upper port, three switches (S_{A1}, S_{A2}, and S_{A4}) experience $2I$ instantaneous current at most and a switch (S_{A3}) passes I instantaneous current. In the same way, when the grid is connected to the lower port, three switches (S_{A1}, S_{A3}, and S_{A4}) experience $2I$ instantaneous current at most and a switch (S_{A2}) passes I instantaneous current. Nevertheless, when the grid is connected to the middle port, two middle switches (S_{A2} and S_{A3}) experience $2I$ while the two corner switches (S_{A1} and S_{A4}) experience I instantaneous current at most. Therefore, the best port for grid connection in terms of total required current rating for the UEPC is the middle port. However, when the grid is connected to the lower and upper ports, the total required current rating for the UEPC is the same. It is worth mentioning that with the same total current rating in AC-AC-AC and AC-AC-DC configurations, larger amount of power can be handled by later configuration. For instance, if the nominal power of all AC-based and DC-based RESs is considered equal to P, in the AC-AC-AC configuration $2P$ active power can be delivered to the grid at most but in the AC-AC-DC configuration, the maximum delivered active power can reach $4P$. This is a remarkable advantage of the AC-AC-DC configuration compared with the AC-AC-AC one.

TABLE 2 Maximum required current rating of a three-port version of UEPC for grid integration of two RESs

	S_{A1} = OFF	S_{A2} = OFF	S_{A3} = OFF	S_{A4} = OFF	*Max.*
Grid is connected to upper port					
i_{SA1}	0	$2I$	I	0	$2I$
i_{SA2}	$-2I$	0	$-I$	$-2I$	$2I$
i_{SA3}	$-I$	I	0	$-I$	I
i_{SA4}	0	$2I$	I	0	$2I$
Total required rating					$7I$
Grid is connected to middle port					
i_{SA1}	0	$-I$	I	0	I
i_{SA2}	I	0	$2I$	I	$2I$
i_{SA3}	$-I$	$-2I$	0	$-I$	$2I$
i_{SA4}	0	$-I$	I	0	I
Total required rating					$6I$
Grid is connected to lower port					
i_{SA1}	0	$-I$	$-2I$	0	$2I$
i_{SA2}	I	0	$-I$	I	I
i_{SA3}	$2I$	I	0	$-2I$	$2I$
i_{SA4}	0	$-I$	$-2I$	0	$2I$
Total required rating					$7I$

4 | POWER LOSS EVALUATION

The power loss in the unified converter is classified into two categories (a) switching loss and (b) conduction loss. When switch is being turned on and off, the switching loss depends on the blocked voltage and the flowing current. Since in both configurations, sources with the same nominal current are connected to the ports and DC-link voltage is also the same, the switching loss in both configurations is almost equal. However, as the conduction loss highly depends on the root-mean-square (RMS) switch current, the conduction loss difference can be considerable and needs to be evaluated in detail. According to [9, 17, 18] and the following equation given in [20, 21], the conduction loss of the semiconductors depends on ON-resistance and RMS current.

$$P_{Co} = V_{CE} \times i_{RMS} + R_{CE} \times i_{RMS}^2, \quad (1)$$

where V_{CE} is the drop voltage across the switch during conduction, P_{Co} is the conduction loss, and R_{CE} is ON-resistance of the switch. Using the same ON-resistance for both configurations, it is concluded that the conduction losses can be compared using the RMS current. Considering the instantaneous current shown in Table 1, the RMS switch current difference between two configurations for power switching devices in phase A (S_{A1}, S_{A2}, S_{A3}, and S_{A4}) can be, respectively, expressed as follows:

$$\Delta i_{RMS}^2\Big|_{S_{A1}} = \frac{1}{T}\int \left[(i_{S1}+i_G+I_{DC})^2-(i_{S1}+i_G+i_{S2})^2\right] \times \frac{T_1}{T}dt, \tag{2}$$

$$\Delta i_{RMS}^2\Big|_{S_{A2}} = \frac{1}{T}\int \left[(i_G+I_{DC})^2-(i_G+i_{S2})^2\right] \times \frac{T_2}{T}dt, \tag{3}$$

$$\Delta i_{RMS}^2\Big|_{S_{A3}} = \frac{1}{T}\int \left[(I_{DC})^2-(i_{S2})^2\right] \times \frac{T_3}{T}dt, \tag{4}$$

$$\Delta i_{RMS}^2\Big|_{S_{A4}} = \frac{1}{T}\int \left[(i_{S1}+i_G+I_{DC})^2-(i_{S1}+i_G+i_{S2})^2 +(i_G+I_{DC})^2-(i_G+i_{S2})^2+(I_{DC})^2 -(i_{S2})^2\right] \times \frac{T_4}{T}dt, \tag{5}$$

where i_{S1} is the upper AC source current, i_G is the grid-side current, i_{S2} is the lower AC source current, and I_{DC} is DC source current. The total RMS switch current difference between two configurations Δi_{RMS}^2 can be then written by:

$$\Delta i_{RMS}^2 = \Delta i_{RMS}^2\Big|_{S_{A1}} + \Delta i_{RMS}^2\Big|_{S_{A2}} + \Delta i_{RMS}^2\Big|_{S_{A3}} + \Delta i_{RMS}^2\Big|_{S_{A4}}. \tag{6}$$

It is noted that only phase A is taken into account for power loss evaluation. For phase B and C, the same analysis can be used. To obtain a general loss evaluation, frequency and phase of AC sources are considered different. Therefore, the instantaneous current of every source is defined as follows:

$$i_{S1} = I_{S1}cos(\omega_{S1}t+\phi_{S1}), \tag{7}$$

$$i_G = I_G cos(\omega_G t), \tag{8}$$

$$i_{S2} = I_{S2}cos(\omega_{S2}t+\phi_{S2}), \tag{9}$$

$$I_{DC} = I_{dc}, \tag{10}$$

where I_{S1}, ω_{S1}, and ϕ_{S1} are the amplitude, angular frequency, and phase of upper AC source current, I_{S2}, ω_{S2}, and ϕ_{S2} are the amplitude, angular frequency, and phase of lower AC source current, I_G and ω_G are the amplitude and angular frequency of the grid-side current, respectively. The time interval assigned to every switching state brought in Table 1, is written based on the reference waveform as follows:

$$T_1 = 0.5T_s(1-Ref_{S1}), \tag{11}$$

$$T_2 = 0.5T_s(Ref_{S1}-Ref_G), \tag{12}$$

$$T_3 = 0.5T_s(Ref_G-Ref_D), \tag{13}$$

$$T_3 = 0.5T_s(1+Ref_D), \tag{14}$$

where T_s is switching period and Ref_{S1}, Ref_G, Ref_D are the modulation references of upper, middle, and lower ports, respectively, and expressed as follows:

$$Ref_{S1} = M_{S1}cos(\omega_{S1}+\phi_{S1})+\mu_{S1}, \tag{15}$$

$$Ref_G = M_G cos(\omega_G+\phi_G)+\mu_G, \tag{16}$$

$$Ref_D = \begin{cases} M_{S2}cos(\omega_{S2}+\phi_{S2})+\mu_{S2} & AC-AC-AC \\ \mu_{dc} & AC-AC-DC \end{cases}, \tag{17}$$

where M_{S1}, M_G, and M_{S2} are the modulation indices of the upper AC source, grid, and lower AC source, respectively. μ_{S1}, μ_G, μ_{S2}, and μ_{dc} are the dc offsets applied to the modulation references of different ports, respectively. To provide a fair comparison, dc offsets applied to modulation indices of lower AC and DC sources are considered as follows:

$$\mu_{dc} = \mu_{S2}. \tag{18}$$

By substituting (7)–(17) into (2)–(5), the RMS switch current difference between two configurations can be re-written by:

$$\Delta i_{RMS}^2\Big|_{S_{A1}} = (1-\mu_{S1})(2I_{dc}^2-I_{S2}^2)-2M_{S1}I_{S1}I_{dc}, \tag{19}$$

$$\Delta i_{RMS}^2\Big|_{S_{A2}} = (\mu_{S1}-\mu_G)(2I_{dc}^2-I_{S2}^2)-2M_G I_G I_{dc}, \tag{20}$$

$$\Delta i_{RMS}^2\Big|_{S_{A3}} = (\mu_G-\mu_{S2})(2I_{dc}^2-I_{S2}^2), \tag{21}$$

$$\Delta i_{RMS}^2\Big|_{S_{A4}} = 3(1+\mu_{S2})(2I_{dc}^2-I_{S2}^2). \tag{22}$$

Considering $I_{S1}=I_{S2}=I_{dc}=I$ and $I_G=2I$, the total RMS current difference between two configurations can be expressed as follows:

$$\Delta i_{RMS}^2 = (-4M_G-2M_{S1}+2\mu_{dc}+4)I. \tag{23}$$

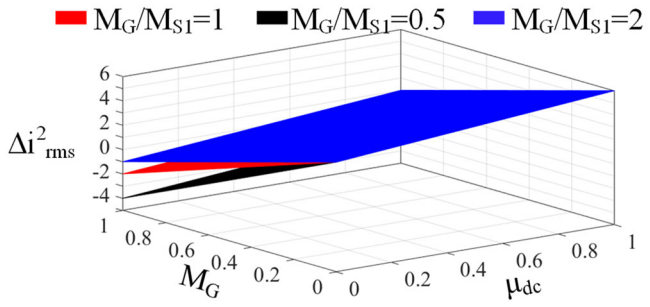

FIGURE 4 Loss comparison of configurations when $I_{S1} = I_{S2} = I_{dc} = I$ and $I_G = 2I$

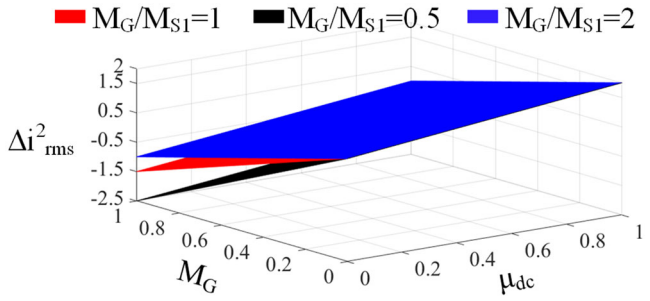

FIGURE 5 Loss comparison of configurations when $I_{S2} = I_{dc} = I$, $I_{S1} = 2I$, and $I_G = 3I$

The conduction loss in AC-AC-DC configuration is lower than AC-AC-AC configuration if $\Delta i^2_{RMS} \leq 0$.

The area of lower RMS switch current for AC-AC-DC configuration compared to AC-AC-AC configuration when $I_{S1} = I_{S2} = I_{dc} = I$ and $I_G = 2I$ is depicted in Figure 4. As can be seen, the RMS current and therefore the conduction loss difference between configurations, depend on modulation index of various ports so that for some modulation indices the power loss of AC-AC-DC is lower than AC-AC-AC. When RESs with different nominal power ratings are connected to the unified structure, the same analysis can be made. As it is shown in Figures 5 and 6, there are several modulation indices leading to a lower RMS switch current, and therefore, the conduction loss in the AC-AC-DC configuration.

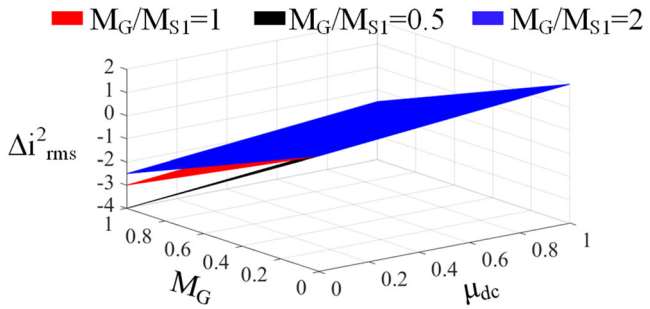

FIGURE 6 Loss comparison of configurations when $I_{S1} = I$, $I_{dc} = I_{S2} = 2I$, and $I_G = 3I$

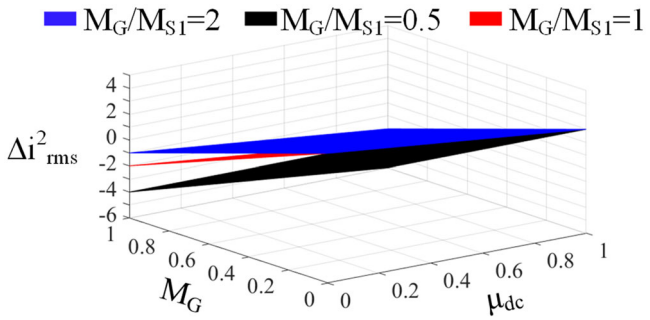

FIGURE 7 Loss comparison of configurations when $I_{S1} = I_{S2} = I_{dc} = I$ and $I_G = 2I$

In the AC-AC-AC configuration, two AC sources with the same specifications might be connected to the upper and lower ports. Considering the same magnitude, frequency and phase for PMSGs' currents, the RMS switch current difference for each semiconductor in phase A can be re-written as follows:

$$\Delta i^2_{RMS}\Big|_{S_{A1}} = -2M_{S1}I_{S1}I_{dc} + (1-\mu_{S1})(2I^2_{dc} + 2I^2_{S1} - I^2_{S2}), \tag{24}$$

$$\Delta i^2_{RMS}\Big|_{S_{A2}} = (\mu_{S1} - \mu_G)(2I^2_{dc} - I^2_{S2}) - 2M_G I_G I_{dc}, \tag{25}$$

$$\Delta i^2_{RMS}\Big|_{S_{A3}} = (\mu_G - \mu_{S2})(2I^2_{dc} - I^2_{S2}), \tag{26}$$

$$\Delta i^2_{RMS}\Big|_{S_{A4}} = (6I^2_{dc} - 2I^2_{S1} - 3I^2_{S2})(1+\mu_{S2}). \tag{27}$$

The total RMS switch current difference when $I_{S1} = I_{S2}$ and $\mu_{S1} = \mu_{S2} = \mu_{dc}$ can be expressed by:

$$\Delta i^2_{RMS} = -2M_{S1}I_{S1}I_{dc} - 2M_G I_G I_{dc} + 8I^2_{dc} - 4I^2_{S1} + 4\mu_{S1}I^2_{dc} - 6\mu_{S1}I^2_{S1}. \tag{28}$$

If $I_{S1} = I_{S2} = I_{dc} = I$ and $I_G = 2I$, (28) can be simplified as:

$$\Delta i^2_{RMS} = (-2M_{S1} - 4M_G)I^2 + (4 - 2\mu_{S1})I^2. \tag{29}$$

The area in which the power loss of the AC-AC-DC configuration is lower than the AC-AC-AC one, considering different values for $\frac{M_G}{M_{S1}}$, is shown in Figure 7.

In the AC-AC-DC configuration, according to [14], the effect of DC source's duty cycle on the instantaneous current depends on type of the connected DC source/load. In the case of connecting a photovoltaic system, the DC port acts as a boost converter. Therefore, the inductance current flowing through the switches can be expressed in terms of modulation index as follows:

$$I_{dc} = I_L = \frac{V_{DC}}{(1-\mu_{dc})R_{DC}}, \tag{30}$$

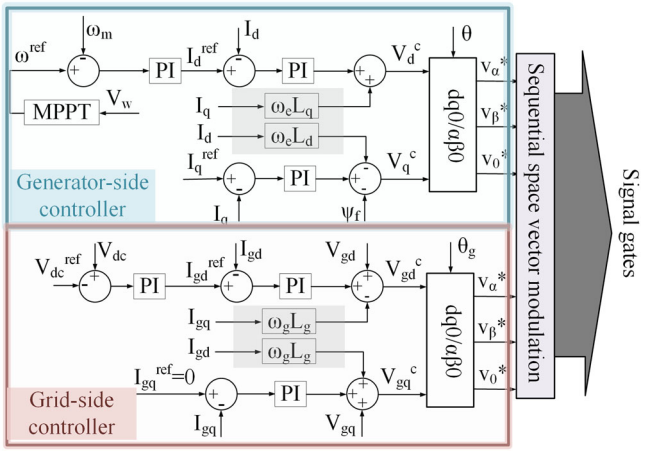

FIGURE 8 The designed control strategy for generator and grid side ports in AC-AC-AC configuration

where V_{DC} is DC-link voltage, I_L is the average current of DC port's inductance, and R_{DC} is the equivalent resistor seen from DC-link. As can be seen, the inductance current (DC port current), and therefore, the instantaneous current directly depends on DC port's duty cycle. This means that an increase in the duty cycle leads to an increase in the instantaneous current.

5 | RESULTS AND DISCUSSION

5.1 | Power flow evaluation

5.1.1 | AC-AC-AC configuration

In the AC-AC-AC configuration, as shown in Figure 2(a), two AC-based RESs are connected to the upper and lower ports while the grid is connected to the middle port. The generated power by RESs is simultaneously injected to DC-bus and then delivered to the grid through grid-side port. Due to the flexibility of the compact structure, one of the AC sources can be replaced with an AC load. In this case, the demanded power by AC load can be either provided by AC source or grid through DC-bus. Two PMSG-based WESs are considered to be integrated into the grid using compact structure, where the upper and lowers ports are working as generator-side converters.

The designed control strategy in synchronous frame for PMSGs and grid is shown in Figure 8. The speed control of the generator for capturing maximum power from the wind is performed by adjusting direct current component. However, the quadrature component is responsible for controlling the reactive power and guaranteeing the unity power factor in the grid side. The simulation results when different wind speed patterns are applied to the PMSGs are demonstrated in Figure 9. As can be seen, both PMSGs are perfectly controlled so that their rotational speeds are properly following the reference values provided by maximum power point tracking (MPPT) subsystem.

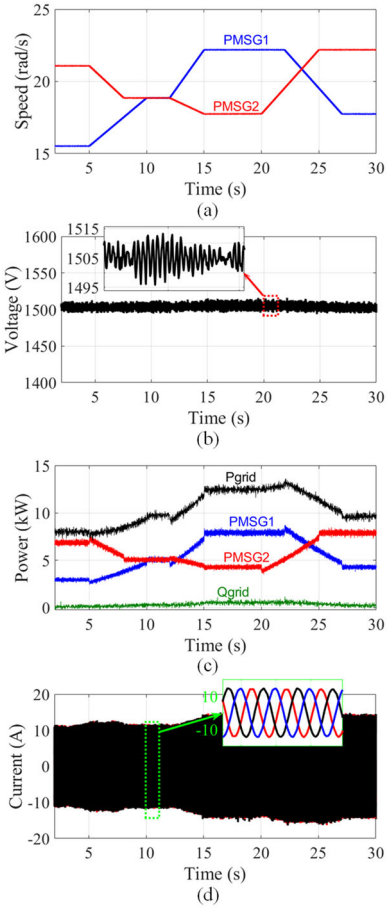

FIGURE 9 Simulation results for AC-AC-AC configuration, (a) PMSGs' speed, (b) DC-bus voltage, (c) power flow, and (d) grid-side current

As shown in Figure 9(b), the grid port is also controlled well in a way that DC-bus voltage is effectively regulated, which leads to a excellent power flow between sources as illustrated in Figure 9(c). The grid-side three-phase currents are also presented in Figure 9(d).

5.1.2 | AC-AC-DC

In the second configuration, as shown in Figure 2(b), the lower ports of different phases can be utilized to interface with DC-based sources, loads, and energy storage systems. Depending on the number of integrated DC-sources (can be equal to the number of phases or not), the sequential space vector modulation should be adapted [14]. Apart from PMSG-based WES and grid-side ports, three solar energy systems (one in each phase) are interconnected by compact structure to verify the AC-AC-DC configuration. In this case, DC ports work as boost converters and step up the output voltage of the panels to reach DC-bus voltage. The duty cycle of every port is controlled in a way that the maximum power can be extracted from the connected panel as presented in Figure 10. For PMSG and grid-side ports, the same control strategy as shown in Figure 9 is exploited. The simulation results carried out by MATLAB/Simulink when

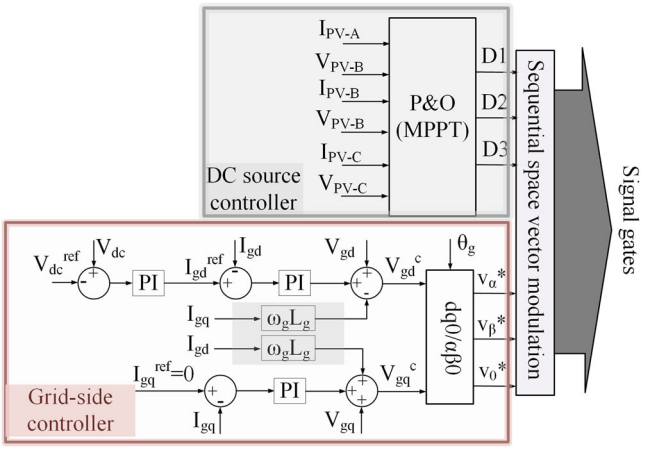

FIGURE 10 The designed control strategy for solar and grid side ports in AC-AC-DC configuration

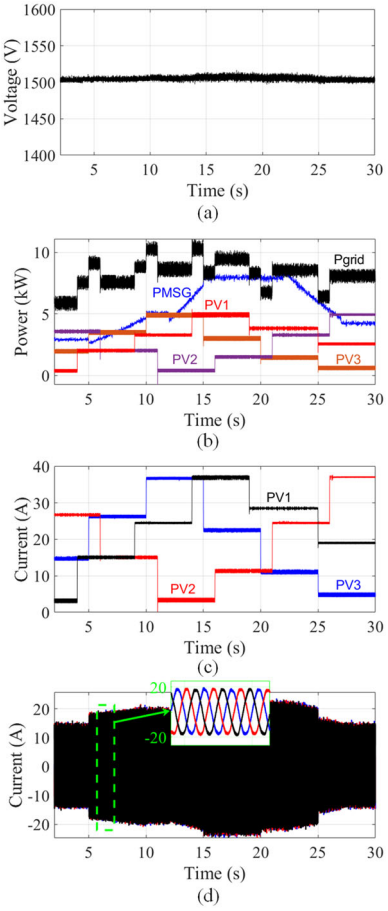

FIGURE 11 Simulation results for AC-AC-DC configuration, (a) DC-bus voltage, (b) power flow, (c) panels' currents, and (d) grid-side current

solar panels experience different irradiation profiles are demonstrated in Figure 11. The effective performance of grid-side port is shown in Figure 11(a), where the DC-bus voltage is appropriately controlled regardless of high number of integrated RESs. The power flow between RESs and the grid is presented in Figure 11(b). As can be seen, the delivered active power to the grid

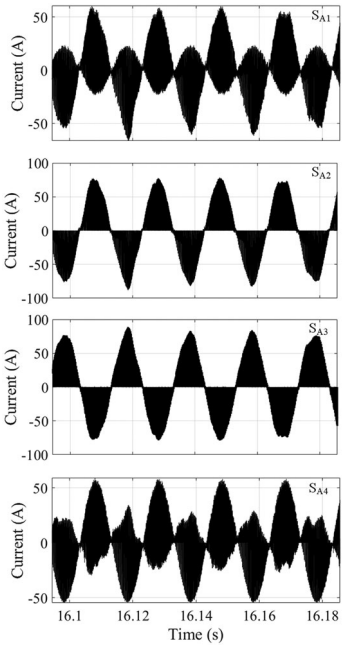

FIGURE 12 Instantaneous currents flowing through power switching devices in phase A for AC-AC-AC configuration

is equal to the summation of produced power by RESs. Though the DC ports experience different duty cycles, the DC sources' currents are decently adjusted to obtain maximum power from panels (see Figure 11(c)). The grid-side current in this configuration is also demonstrated in Figure 11(d). Compared to the grid-side current of the AC-AC-AC configuration depicted in Figure 9(d), larger current can be injected into the grid because two more RESs are integrated in the AC-AC-DC configuration. In other words, with the same current rating for power switching devices, the larger amount of active power can be handled by AC-AC-DC configuration.

5.2 | Current stress analysis

5.2.1 | AC-AC-AC configuration

The instantaneous currents flowing through power switching devices in phase A when two PMSGs with the same specifications are connected to upper and lower ports and the grid is located in the middle port, are shown in Figure 12. As can be seen, the upper and lower switches are almost experiencing the same instantaneous current. The middle switches (S_{A2} and S_{A3}), are also carrying the similar instantaneous currents.

5.2.2 | AC-AC-DC configuration

The instantaneous currents flowing through semiconductor switches in phase A for AC-AC-DC configuration are shown

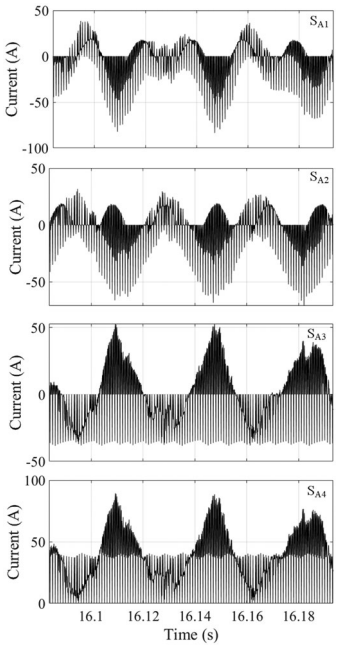

FIGURE 13 Instantaneous currents flowing through power switching devices in phase A for AC-AC-DC configuration

in Figure 13. In this case, a solar energy system with a nominal power of 7kW is connected to the lower port. However, the upper and middle ports are utilized to connect PMSG and grid, respectively. The effects of lower port duty cycle on instantaneous currents are obvious. As can be seen, the first and last two switches have similar instantaneous currents.

6 | CONCLUSION

In this paper, a current stress and switching loss evaluation for a unified expandable power converter is presented. Considering both feasible AC-AC-AC and AC-AC-DC configurations, the instantaneous current flowing trough every switch in each valid switching state is calculated. The total required current rating for a three-port version of UEPC considering various ports for grid-connection is also obtained. The analysis revealed that if grid is connected to the middle port, the minimum current rating for semiconductors in leg A is required. It is also obtained that the AC-AC-DC configuration is able to handle higher amount of power considering the same current rating for power switching devices in both configurations. The conduction loss difference between AC-AC-AC and AC-AC-DC configurations is explicitly assessed. It is successfully demonstrated that there are some modulation indices that result in a lower switching loss in the AC-AC-DC configuration compared to the AC-AC-AC configuration. The power flow capability of both configurations was finally verified by simulations results. It is shown that both configurations are properly able to mange the power flow between different ports so that the maximum power can be produced by RESs. The AC-AC-DC configuration, however, provides off-grid operating mode due to its capability in integration of energy storage systems.

ORCID

Hamed Bizhani https://orcid.org/0000-0001-5458-8039
S. M. Muyeen https://orcid.org/0000-0003-4955-6889
Kuaanan Techato https://orcid.org/0000-0002-9178-8416
Lazhar Ben-Brahim https://orcid.org/0000-0003-4510-8544
Frede Blaabjerg https://orcid.org/0000-0001-8311-7412

REFERENCES

1. Pudjianto, D., et al.: Virtual power plant and system integration of distributed energy resources. IET Renewable Power Gener. 1(1), 10–16 (2007)
2. Ssekulima, E.B., et al.: Wind speed and solar irradiance forecasting techniques for enhanced renewable energy integration with the grid: a review. IET Renew. Power Gener. 10(7), 885–989 (2016)
3. Singh, S., et al.: Optimal power scheduling of renewable energy systems in microgrids using distributed energy storage system. IET Renew. Power Gener. 10(9), 1328–1339 (2016)
4. Ali, L., et al.: Optimal planning of clustered microgrid using a technique of cooperative game theory. Electr. Power Syst. Res. 183, 106262 (2020)
5. Rostami, S., et al.: Three-port dc–dc converter based on quadratic boost converter for stand-alone PV/battery systems. IET Power Electron. 13(10), 2106–2118 (2020)
6. Shahbazi, M., et al.: Five-leg converter topology for wind energy conversion system with doubly fed induction generator. Renewable Energy 36(11), 3187–3194 (2011)
7. Heydari, M., et al.: A novel variable-speed wind energy system using permanent-magnet synchronous generator and nine-switch ac/ac converter. In: 2011 2nd Power Electronics, Drive Systems and Technologies Conference, pp. 5–9. IEEE, Piscataway (2011)
8. Ajami, A., et al.: Design and control of a grid tied 6-switch converter for two independent low power wind energy resources based on PMSGs with MPPT capability. Renew. Energy 87, 532–543 (2016)
9. Loh, P.C., et al.: Compact integrated energy systems for distributed generation. IEEE Trans. Ind. Electron. 60(4), 1492–1502 (2012)
10. Banaei, M.R., Dehghanzadeh, A.R.: Wind farm based doubly fed induction generator using a novel ac/ac converter. In: 2011 2nd Power Electronics, Drive Systems and Technologies Conference, pp. 398–402. IEEE, Piscataway (2011)
11. Wang, K., et al.: Modeling of nine-switch-converter based on virtual-leg and its application in dfig wind generation system. IEEE Trans. Power Electron. 35(7), 7674–7688 (2019)
12. Azizi, M., et al.: A new family of multi-input converters based on three switches leg. IEEE Trans. Ind. Electron. 63(11), 6812–6822 (2016)
13. Bizhani, H., et al.: Wind farm grid integration architecture using unified expandable power converter. IEEE Trans. Power Electron. 34(4), 3407–3417 (2018)
14. Bizhani, H., et al.: A grid-connected smart extendable structure for hybrid integration of distributed generations. IEEE Access 7, 105235–105246 (2019)
15. Bhattacharjee, A.K., et al.: Review of multiport converters for solar and energy storage integration. IEEE Trans. Power Electron. 34(2), 1431–1445 (2018)
16. Chen, Y.M., et al.: Multi-input inverter for grid-connected hybrid pv/wind power system. IEEE Trans. Power Electron. 22(3), 1070–1077 (2007)
17. Ali, K., et al.: A special application criterion of the nine-switch converter with reduced conduction loss. IEEE Trans. Ind. Electron. 65(4), 2853–2862 (2017)
18. Qin, Z., et al.: Application criteria for nine-switch power conversion systems with improved thermal performance. IEEE Trans. Power Electron. 30(8), 4608–4620 (2014)

19. Bizhani, H., et al.: Dual mechanical port machine based hybrid electric vehicle using reduced switch converters. IEEE Access 7, 33665–33676 (2019)
20. Bierhoff, M.H., Fuchs, F.W.: Semiconductor losses in voltage source and current source IGBT converters based on analytical derivation. In: 2004 IEEE 35th Annual Power Electronics Specialists Conference (IEEE Cat. No. 04CH37551). vol. 4, pp. 2836–2842. IEEE, Piscataway (2004)
21. Dehghan, S.M., et al.: Hybrid electric vehicle based on bidirectional z-source nine-switch inverter. IEEE Trans. Veh. Technol. 59(6), 2641–2653 (2010)

How to cite this article: Bizhani H, Muyeen SM, Tatari FR, Techato K, Ben-Brahim L, Blaabjerg F. Current stress and switching loss evaluation of a unified expandable power converter used for grid-integration of renewable energy sources. IET Renew. Power. Gener. 2021;15:2561–2570.
https://doi.org/10.1049/rpg2.12148